NASA TN D-1166

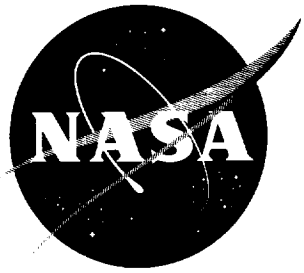

TECHNICAL NOTE

D-1166

A COMPARISON OF REVERSE-FEED AND POROUS-TUNGSTEN ION ENGINES

By Thaine W. Reynolds and J. Howard Childs

Lewis Research Center
Cleveland, Ohio

NATIONAL AERONAUTICS AND SPACE ADMINISTRATION
WASHINGTON February 1962

NATIONAL AERONAUTICS AND SPACE ADMINISTRATION

TECHNICAL NOTE D-1166

A COMPARISON OF REVERSE-FEED AND POROUS-TUNGSTEN ION ENGINES

By Thaine W. Reynolds and J. Howard Childs

SUMMARY

A comparison of the theoretical performance of reverse-feed and porous-tungsten cesium ion engines is made considering (1) power efficiency, (2) propellant utilization efficiency, (3) current densities, (4) emitter temperature, and (5) charge exchange, at specific-impulse levels of 3000 to 10,000 seconds.

The porous-tungsten engine becomes better as the pore size becomes smaller and the fractional open area increases. For small pore size (1 to 2 microns), the porous-tungsten engine has better propellant utilization efficiency than the reverse-feed engine. Charge exchange currents are lower for the porous-tungsten engine at low power efficiencies. At higher power efficiencies, however, the charge exchange currents are comparable for the two engine types.

Higher power efficiency can be attained with the reverse-feed engine for any given level of current density, or the same power efficiency can be attained at lower current density levels with the reverse-feed system than with the porous-tungsten engine. If porous-tungsten engines can be operated at extremely high values of current density so as to achieve high power efficiencies, then the propellant utilization efficiency decreases, and in some cases becomes comparable with the utilization efficiency of the reverse-feed engines.

INTRODUCTION

Because of the capabilities of electric propulsion for space flight, there is currently considerable effort going into the research and development of electric propulsion devices. One class of such devices is the electrostatic ion engine which employs contact ionization of the propellant on a heated surface to produce the ions. There are essentially two types of engines employing contact ionization which have been investigated to date (ref. 1). These have been classified according to the

manner or direction in which the propellant is introduced onto the ionizing surface. In the reverse-feed system, the propellant is fed back toward the surface, opposite to the direction of the main ion stream; in the through-feed system, the propellant feed flow is from behind the surface, through the porous structure of the ionizing surface material. For the latter type, the almost universal choice has been a porous-tungsten structure made from sintered powder.

The purpose of the present report is to present results of performance analyses of both reverse-feed and porous-tungsten ion engines using tungsten as the surface and cesium as the propellant.

Characteristics of the reverse-feed ion engine are presented in reference 2, wherein the details of the assumptions and calculations are included. These performance characteristics include the flux patterns onto the ionizing surface, propellant efficiency, power efficiency, and the extent to which the ion current will engage in charge exchange reactions with incoming neutrals.

Analysis of the porous-tungsten ion engine is presented in reference 3, wherein the desired pore size for such a purpose is shown to be approximately 1 micron. With pores much above this size, the loss of neutral atoms becomes large and temperature requirements for the emitter become great. Preparation of a porous structure with pores smaller than 1 micron that will retain its permeability at the required temperature levels has not yet been demonstrated. It was also shown that emittance values of the porous surfaces did not reach the low emissivity values of polished tungsten. The word "emittance" is used here to differentiate between an unpolished surface and a polished surface.

The present report, then, draws upon the conclusions of references 2 and 3 to compare the performance at specific-impulse levels of 3000 to 10,000 seconds of the reverse-feed and porous-tungsten ion engines as to (1) power efficiency, (2) propellant utilization efficiencies, (3) current densities, (4) emitter temperature requirements, and (5) the amount of charge exchange occurring.

DESCRIPTION OF ENGINES AND ASSUMPTIONS

The engine models upon which the comparison in this report is based are shown in figure 1. Figure 1(a) shows the reverse-feed system. Cesium propellant is fed onto the ionizing surface through slots in the feed tubes located a distance h downstream from the emitter. As shown in reference 2, the performance of this type of engine varies with, and may be characterized by, the ratio of this distance h to the width of the emitter W_E. The ratio h/W_E is one of the parameters used herein.

The ions formed at the emitter are accelerated to the desired specific impulse by the accelerate-decelerate electrode system of total spacing L from the emitter.

On the basis of the calculations of reference 2, reverse-feed engines selected for comparison in this report assume a ratio of feed distance to emitter width h/W_E from 0.3 to 0.5. The propellant issuing from the feed slot is assumed to spread following a sixth-power cosine law.

In figure 1(b) is shown a through-feed system employing a porous-tungsten ionizer. Here the cesium propellant must pass through the thickness of porous material t_E to reach the ionizing surface. As discussed in reference 3, the important parameters characterizing the performance of the porous-tungsten ionizer are the pore size and the fraction of the total cross section which is open to flow and effective for surface ionization. Two sources are discussed from which ion current might be obtained from porous tungsten: the downstream surface after diffusion across the surface, and the distributed charge inside the pore at the exit plane. The magnitude of the possible current by the latter source would depend upon the extent that the applied field could penetrate into the pores. Since this penetration has not been determined, but is expected to be small, the possible current from this source has not been included in the present analysis. Ion current from surface diffusion only is assumed.

Fractional free cross sections f of 0.1 and 0.2 and pore diameters of 1 and 2 microns are assumed for the porous tungsten engines used for comparison. These numbers represent reasonable ranges of values to be anticipated based on current experience.

POWER EFFICIENCY

The main power loss in a contact ion engine P_R is the power radiated by the hot surface. This loss depends on the emitter temperature and the thermal emittance of the hot surface:

$$\eta_P = \frac{\text{Ion beam power}}{\text{Ion beam power + Radiated power}} = \frac{P_B}{P_B + P_R}$$

$$\eta_P = \frac{1}{1 + \frac{5.73\,\epsilon}{j_{av}V}\left(\frac{T_E}{100}\right)^4}$$

(Symbols are defined and a consistent set of units is given in the appendix.) The temperature to which the surface must be heated T_E to attain high ionization efficiency depends on the current density desired from the surface. When the current density is nonuniform over the surface, as is the case with both the reverse-feed and porous emitter engines, the emitter temperature is determined by the maximum current density encountered rather than by the average current density.

As discussed in reference 4, the power efficiency for a surface with nonuniform current density distribution is related to the power efficiency for uniform flux by the relation

$$\frac{\eta_P}{\eta_{P,0}} = \frac{j_{av}/j_{max}}{\left(\frac{j_{av}}{j_{max}} - 1\right)\eta_{P,0} + 1}$$

This relation applies for surfaces at the same emitter temperature.

The power efficiencies for the porous-tungsten engines, calculated as outlined in reference 4, are shown in figure 2 for a specific impulse of 5000 seconds. Figure 2(a) is for a porous-tungsten structure with 10 percent fractional open area, and figure 2(b) is for one with 20 percent open area. In the calculation of the power efficiency for the porous-tungsten engines, a surface emittance value equal to twice the emissivity of polished tungsten at the same temperature was used (ref. 3). As noted in figure 2, for any given current density the power efficiency increases as the pore size decreases and the fractional open area of the porous tungsten increases.

For power efficiency at specific-impulse values other than 5000 seconds, the following relation is applicable:

$$\eta_P = \frac{1}{1 + \left(\frac{5000}{I_s}\right)^2\left(\frac{1 - \eta_P'}{\eta_P'}\right)}$$

where η_P' is the efficiency at 5000 seconds impulse. This relation is plotted in figure 3 for convenience.

CHARGE EXCHANGE

Ions leaving the emitter are accelerated to the desired final velocity through the accelerate-decelerate electrode system of the engine.

During this travel, the ions pass through surrounding neutral cesium atoms. In the case of the reverse-feed engine, the ions pass through the neutral cesium feed. In the porous-tungsten engine, the neutral cesium density results from the inefficiency of the ionizing source in producing ions. During the travel some of the ions will engage in charge exchanging reactions with the neutral cesium atoms. Since the result of charge-exchange reactions in this case will be ions having improper ion optics, the amount of the charge exchange current which occurs within the electrode system is expected to be related to the amount of ion impingement on the accelerator electrodes. This ion impingement causes accelerator electrode erosion and leads to shortened electrode life. The charge exchange encountered, then, is expected to relate directly to the electrode lifetime.

The fraction of the ion current leaving the emitter which engages in charge exchange reactions is

$$\frac{j_s}{j_{av}} = \sigma_c n_0 L$$

where σ_c is the charge exchange cross section, n_0 is the neutral cesium density, j_s is the secondary ion current produced, and j_{av} is the average primary ion current density.

For the charge exchange calculations presented herein, a constant σ_c of 1×10^{-18} square meter was used for cesium as in reference 2. It is shown in reference 2 for a typical case that, by using theoretical velocity-dependent values of σ_c through the accelerator region, the total charge exchange was reduced to about one-half the value obtained using $\sigma_c = 1 \times 10^{-18}$ square meter. Inasmuch as experimental values of σ_c for cesium are not yet available, it was felt sufficient to make comparisons of performance using the constant σ_c value.

The calculations of charge exchange current density ratio j_s/j_{av} for the reverse-feed engine are presented in reference 2. For the porous-tungsten engine, values of j_s/j_{av} are calculated as follows. The neutral atom density is

$$n_0 = f_n n_p$$

where f_n is the ratio of neutral to charged emitted particle density. Values of f_n are given in reference 3. The ion density at the emitter n_p is given by the relation

$$n_p = \frac{j_{av}}{\left(\frac{\bar{v}}{4}\right)(1.6\times10^{-19})}$$

where $\bar{v}$ is the mean particle velocity at the emitter temperature $\sqrt{8kT_E/\pi m_p}$. Thus,

$$\frac{j_s}{j_{av}} = \frac{\sigma_c L f_n j_{av}}{\left(\frac{\bar{v}}{4}\right)(1.6\times10^{-19})}$$

A value of $L = 2$ millimeters was used, the same as for the reverse-feed engine.

Values of j_s/j_{av} for both porous-tungsten and reverse-feed engines are shown in figure 4 as a function of j_{av}. Charge exchange currents are considerably lower for the porous-tungsten engine over the range of conditions shown in figure 4.

COMPARISON OF PERFORMANCE

The calculated performance of both the reverse-feed and porous-tungsten cesium ion engines is shown in figures 5 to 9.

Figure 5 shows the emitter temperature requirement as a function of the desired average current density. The ideal emitter, since it has uniform coverage and therefore uniform current density over the surface, requires the lowest emitter temperature. The reverse-feed engines with h/W_E in the range 0.3 to 0.5 require slightly higher temperatures, reflecting a moderate nonuniformity in current density distribution. The porous-tungsten engine requires the highest emitter temperature. As the pore size increases or the fractional open area decreases, the required emitter critical temperature increases. These high emitter temperature requirements reflect directly the large surface concentration gradients and, hence, current density variations across the surface of porous-tungsten engines of large pore size.

If for any point on a curve of figure 5 one reads the corresponding current density on the ideal curve at the same temperature, this current density for the ideal emitter is also the maximum current density encountered on the emitter for the actual engine.

Figures 6 to 9 show the various parameters compared on the common basis of power efficiency at four levels of specific impulse. Figure 6 is a plot of average current density against power efficiency. The

reverse-feed engine shows higher power efficiency at all average current density levels of interest. This higher power efficiency for the reverse-feed engine is a result of (a) the lower emittance values associated with the nonporous tungsten surfaces and (b) the more uniform current distribution from the surface with its accompanying lower emitter temperature requirement.

These latter features are shown more strikingly in figure 7, which shows the maximum current density and critical emitter temperature as a function of power efficiency for both engines. The analysis for the porous tungsten ion engines was not continued below about 1300° K, but it may be noted (e.g., fig. 5) that for the smaller pore sizes of interest (1 to 2 microns) the critical temperature requirements are approaching those of the ideal emitter as the current density requirement is lowered. The power efficiencies in figure 7 for the porous-tungsten engine will still be lower than those for the reverse-feed engine at low current densities, however, because of the higher emittance of the porous-tungsten surface.

It is apparent in these figures that the relative performance does not change with specific impulse, but of course the efficiency level increases as specific impulse is raised.

Comparison of the two engine types on the basis of charge exchange currents is shown in figure 8. The porous-tungsten engine has lower charge exchange currents than the reverse-feed engine over the range of conditions included in this comparison. If operation at or below a given level of j_s/j_{av} were desired, for instance, higher power efficiency would be attained with the porous-tungsten engine, as long as the small pore size remained suitable. Charge exchange current increases more rapidly with power efficiency for the porous-tungsten engine, and it might be noted that, if the higher levels of power efficiency were the required operating conditions, the charge exchange currents might be of comparable values. The curves for the porous-tungsten engine in figure 8 were not extended to higher power efficiencies because of the extremely high values of current density that would be required. It might be impossible to operate a porous-tungsten engine under such requirements.

The propellant utilization efficiencies are shown in figure 9 as a function of power efficiency. The porous-tungsten engine has better propellant utilization as long as the comparison is confined to the small pore sizes as shown here (1 to 2 microns) and to lower power efficiencies. In the small pore range the propellant utilization efficiency approaches the equilibrium ionization efficiency for the cesium-tungsten system, as given by the Saha-Langmuir relation. The reverse-feed engine has reduced propellant utilization efficiency due to the propellant that does not reach the emitter initially because of the spread of the cesium

feed from the injector or because of loss of the feed from charge exchange with the ion beam. The propellant flux distribution for the reverse-feed engine was assumed to be that attained with apertures consisting of narrow slots. If better propellant feed systems can be developed, the propellant utilization efficiency for the reverse-feed engine can be increased over values shown in figure 9.

SUMMARY OF RESULTS

Calculations of the performance of reverse-feed and porous-tungsten cesium ion engines gave the following results:

1. The performance of porous-tungsten engines becomes better (power efficiency and propellant utilization efficiency increase, and charge exchange currents decrease) as the pore size becomes smaller and the fractional open area increases. Emitters with pore diameters of 1 micron or less and fractional open areas greater than 20 percent have neither been tested in high-performance ion engines nor checked for sintering at long times at high operating temperature.

The subsequent comments on porous tungsten are restricted to pore sizes in the 1- to 2-micron-diameter range. These values, it should be noted, are more favorable than is characteristic of most material in present use.

2. The porous-tungsten engine is better than the reverse-feed engine on the basis of propellant utilization efficiency or charge exchange current at low and intermediate values of power efficiency. At high power efficiencies, however, the charge exchange currents are comparable for the two engines. At extremely high power efficiencies the propellant utilization efficiency of the porous-tungsten engine decreases and in some cases approaches the values for the reverse-feed engine.

3. Higher power efficiency can be attained with the reverse-feed engine for any given level of current density, or the same power efficiency can be attained at lower current density levels with the reverse-feed system than with the porous-tungsten engine.

4. The required emitter temperature is always higher for the porous-tungsten engine than for the reverse-feed engine. At the higher power efficiencies the difference in emitter temperatures is increased.

Lewis Research Center
National Aeronautics and Space Administration
Cleveland, Ohio, September 18, 1961

APPENDIX - SYMBOLS

(Units of the rationalized mks system are used.)

f	fractional free cross section, dimensionless
f_n	ratio of neutral to charged particle emitted density, dimensionless
h	distance of feed injector hole from emitter face, m
I_s	specific impulse, sec
j_{av}	average current density, amp/m^2
j_{max}	maximum current density, amp/m^2
j_s	secondary current density from charge exchange, amp/m^2
k	Boltzmann constant, joules/^oK
L	length of accelerate-decelerate electrode system, m
m_p	particle mass, kg
n_p	charged particle density, m^{-3}
n_o	neutral particle density, m^{-3}
P_B	ion beam power, w
P_R	power radiated by hot emitter surface, w
T_E	emitter temperature, ^oK
V	total voltage drop of accelerate-decelerate system, v
$\bar{v}$	arithmetic mean particle velocity, m/sec
W_E	emitter width, m
ϵ	surface emittance, dimensionless
η_P	power efficiency, dimensionless
η'_P	power efficiency at specific impulse of 5000 sec, dimensionless

$\eta_{P,0}$ power efficiency of ideal emitter with uniform current density, dimensionless

$\eta_{u,c}$ propellant utilization efficiency corrected for charge exchange, dimensionless

σ_c charge exchange cross section, m^2

REFERENCES

1. Mickelsen, William R.: Electric Propulsion for Space Flight. Aero/Space Eng., vol. 19, no. 11, Nov. 1960, pp. 6-11; 36.

2. Childs, J. Howard: Theoretical Performance of Reverse-Feed Cesium Ion Engines. NASA TN D-876, 1961.

3. Reynolds, Thaine W., and Kreps, Lawrence W.: Gas Flow, Emittance, and Ion Current Capabilities of Porous Tungsten. NASA TN D-871, 1961.

4. Reynolds, Thaine W., and Childs, J. Howard: A Graphical Method for Estimating Ion-Rocket Performance. NASA TN D-466, 1960.

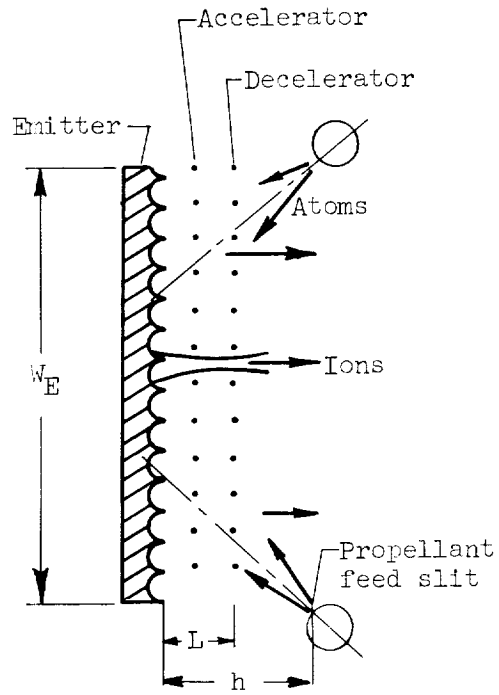

(a) Reverse feed.

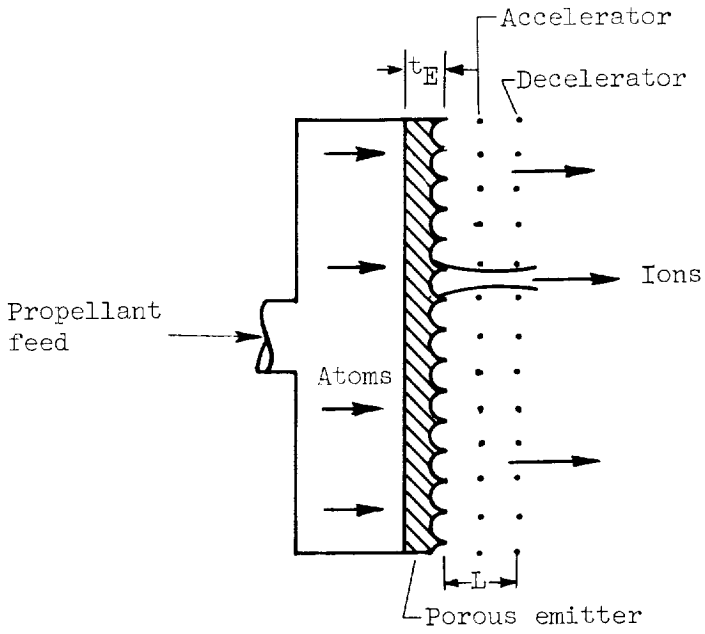

(b) Porous tungsten.

Figure 1. - Engine configurations.

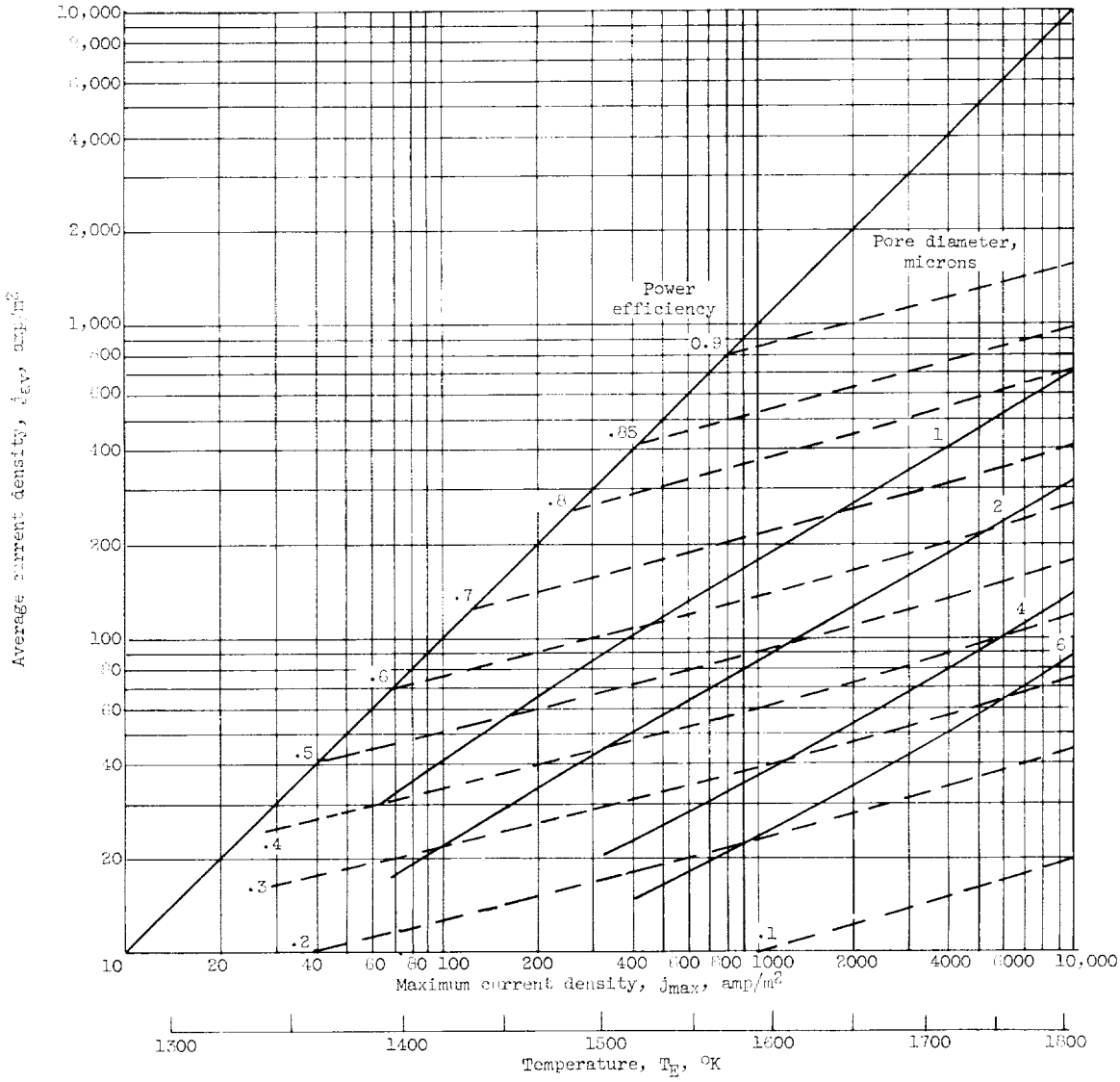

(a) Fractional free cross section, 0.1.

Figure 2. - Power efficiency of porous-tungsten engines. Specific impulse, 5000 seconds.

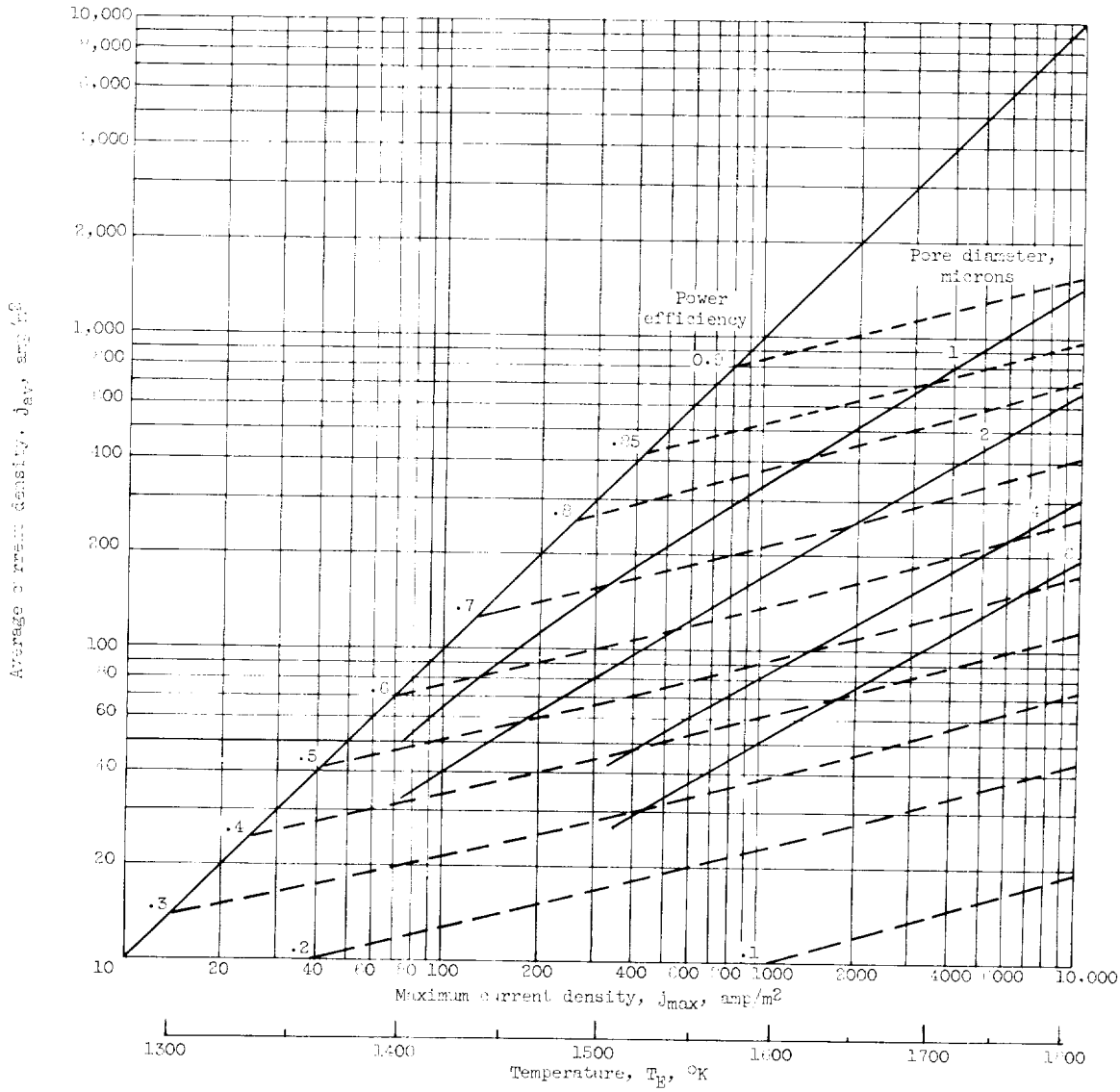

(b) Fractional free cross section, 0.2.

Figure 2. - Concluded. Power efficiency of porous-tungsten engines. Specific impulse, 5000 seconds.

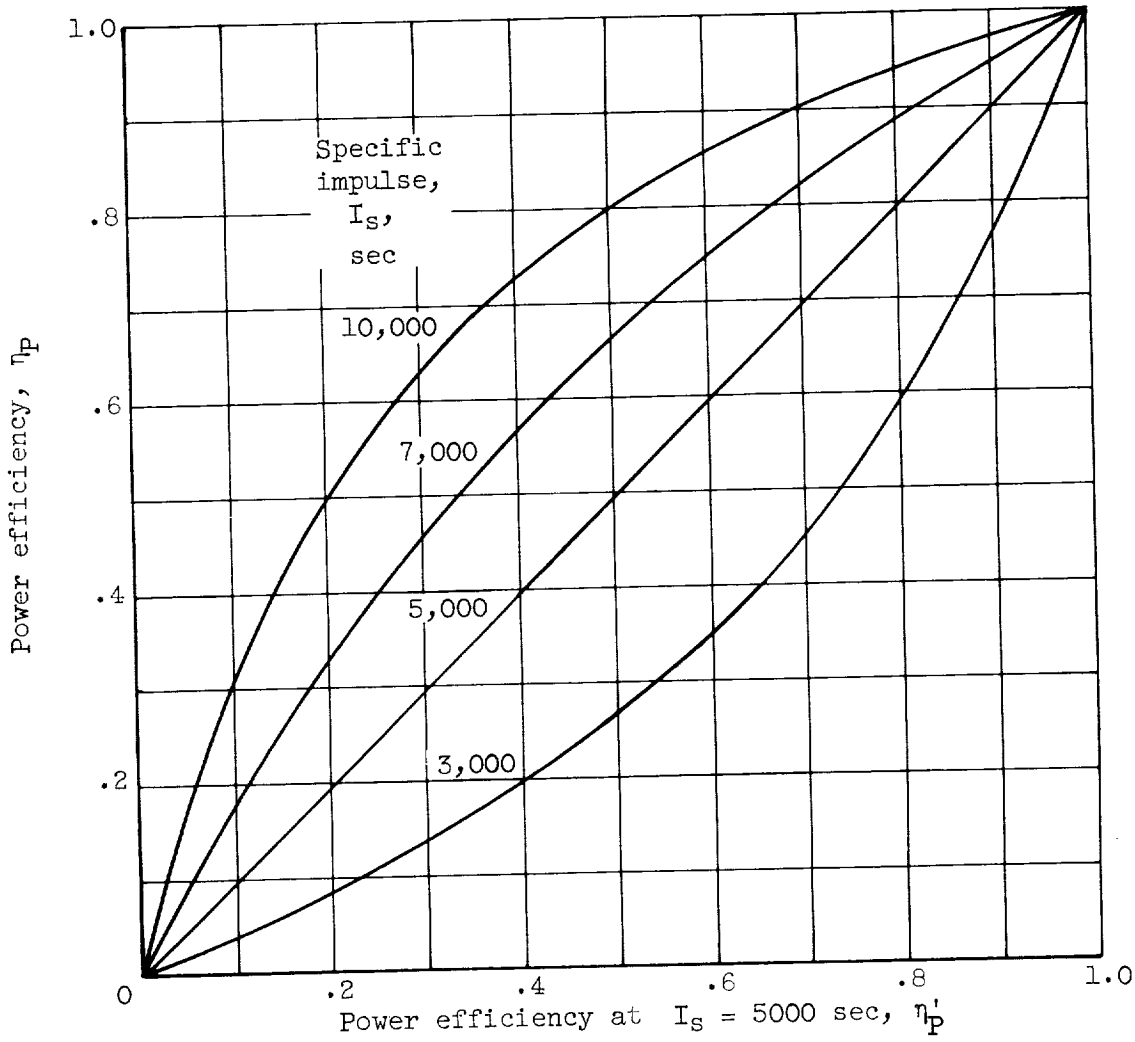

Figure 3. - Variation of power efficiency with specific impulse. $\eta_P = \dfrac{1}{1 + \left(\dfrac{5000}{I_s}\right)^2 \left(\dfrac{1 - \eta'_P}{\eta'_P}\right)}$.

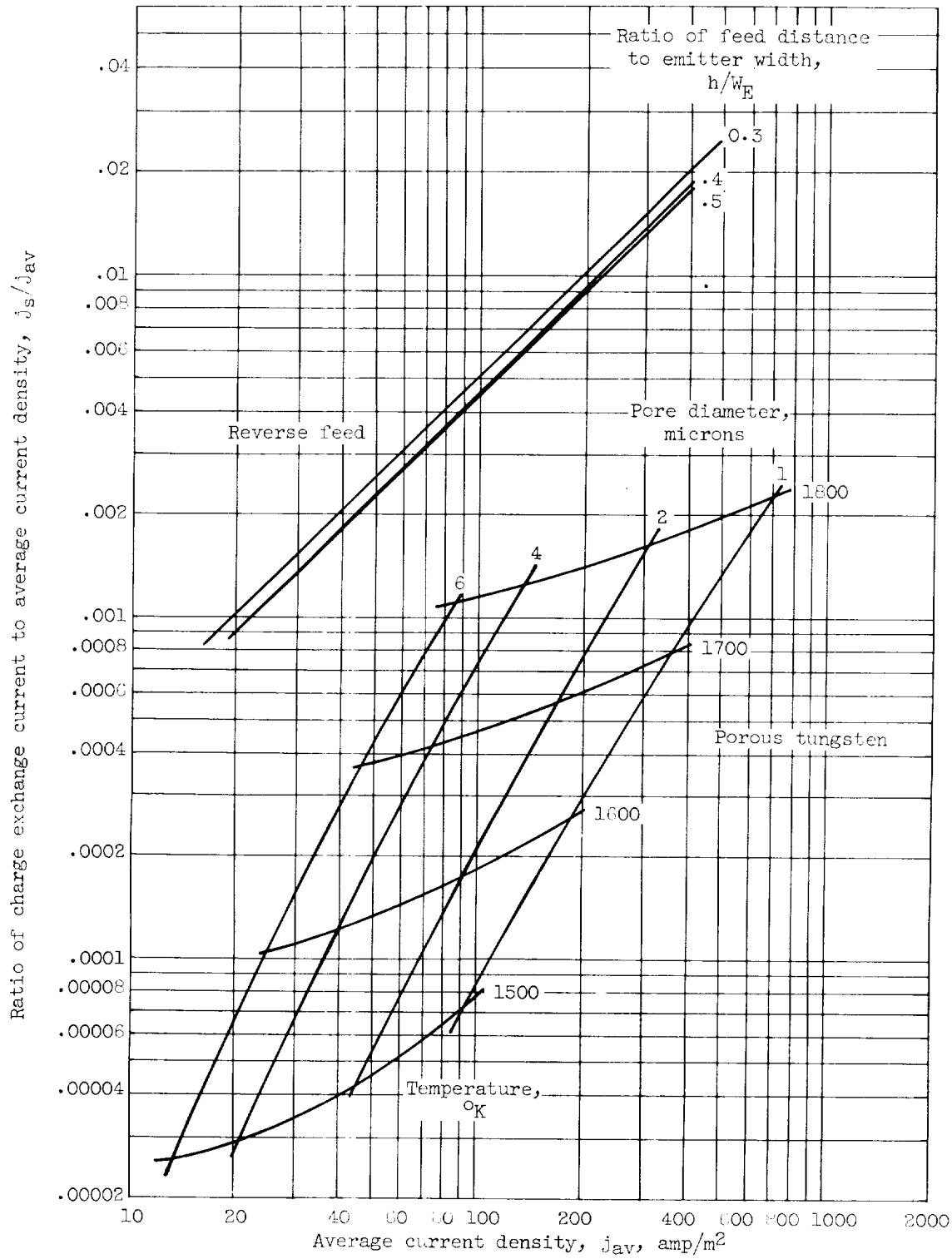

(a) Fractional free cross section, 0.1.

Figure 4. - Charge exchange current density.

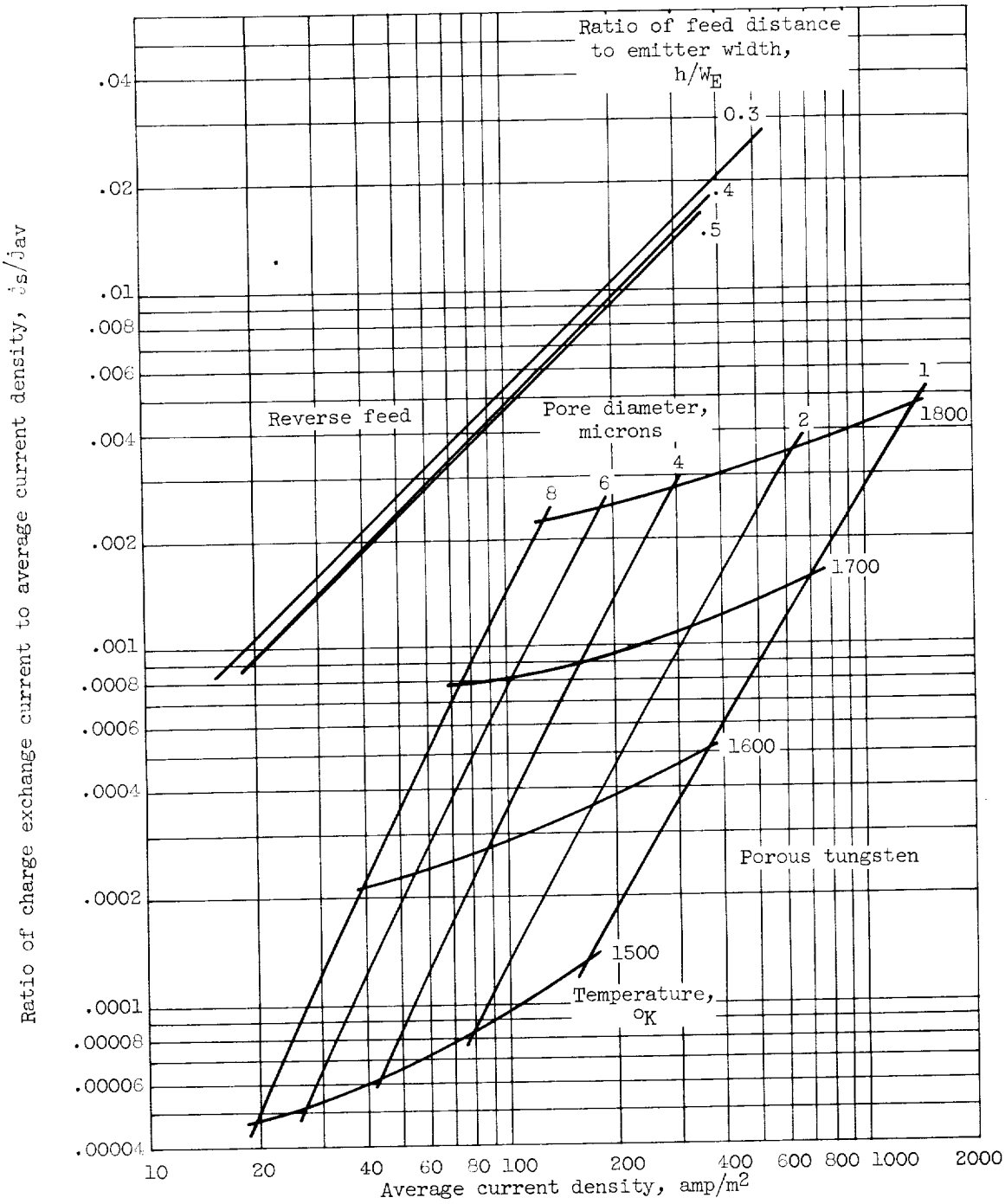

(b) Fractional free cross section, 0.2.

Figure 4. - Concluded. Charge exchange current density.

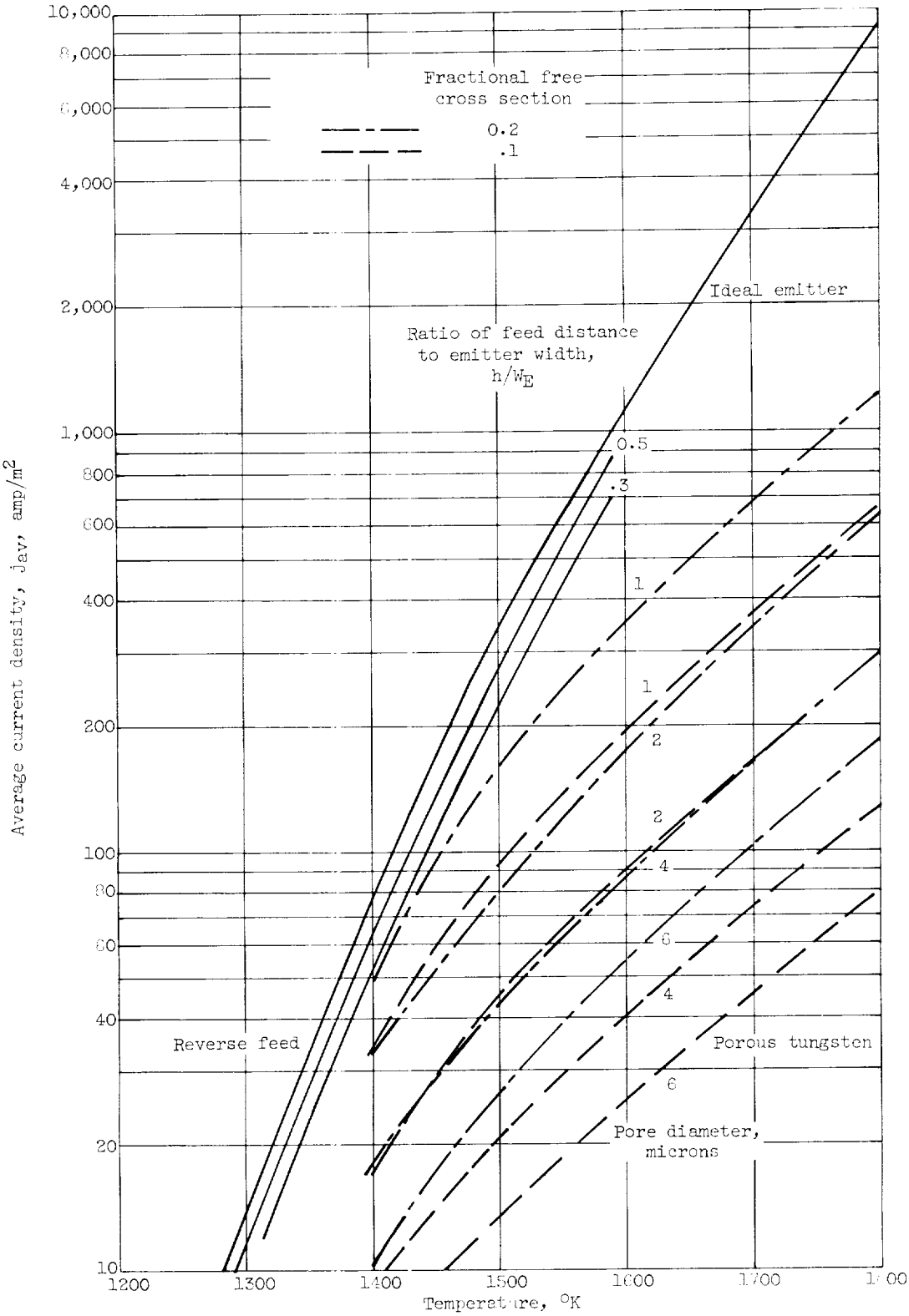

Figure 5. - Variation of average current density with emitter temperature.

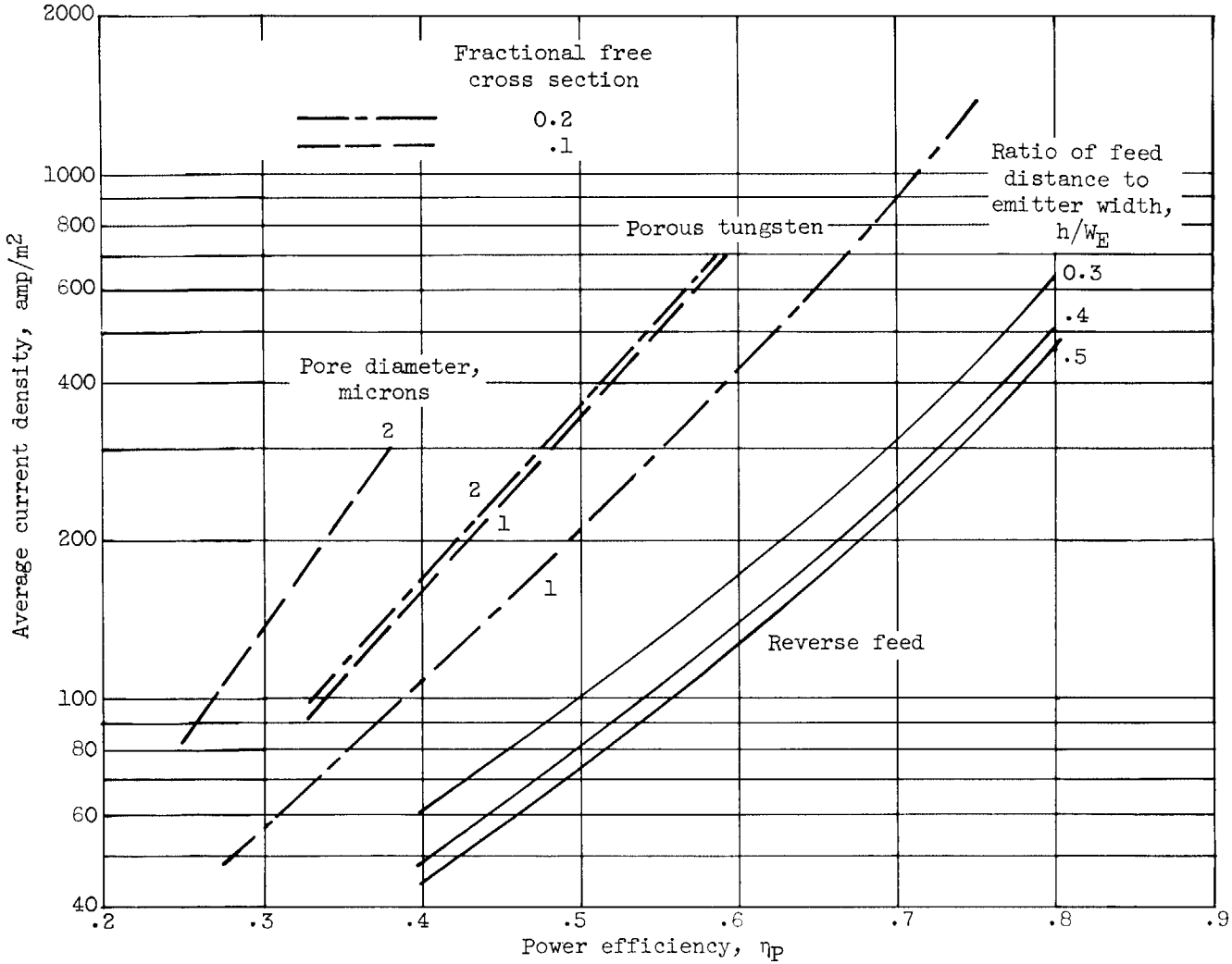

(a) Specific impulse, 3000 seconds.

Figure 6. - Variation of power efficiency with average current density.

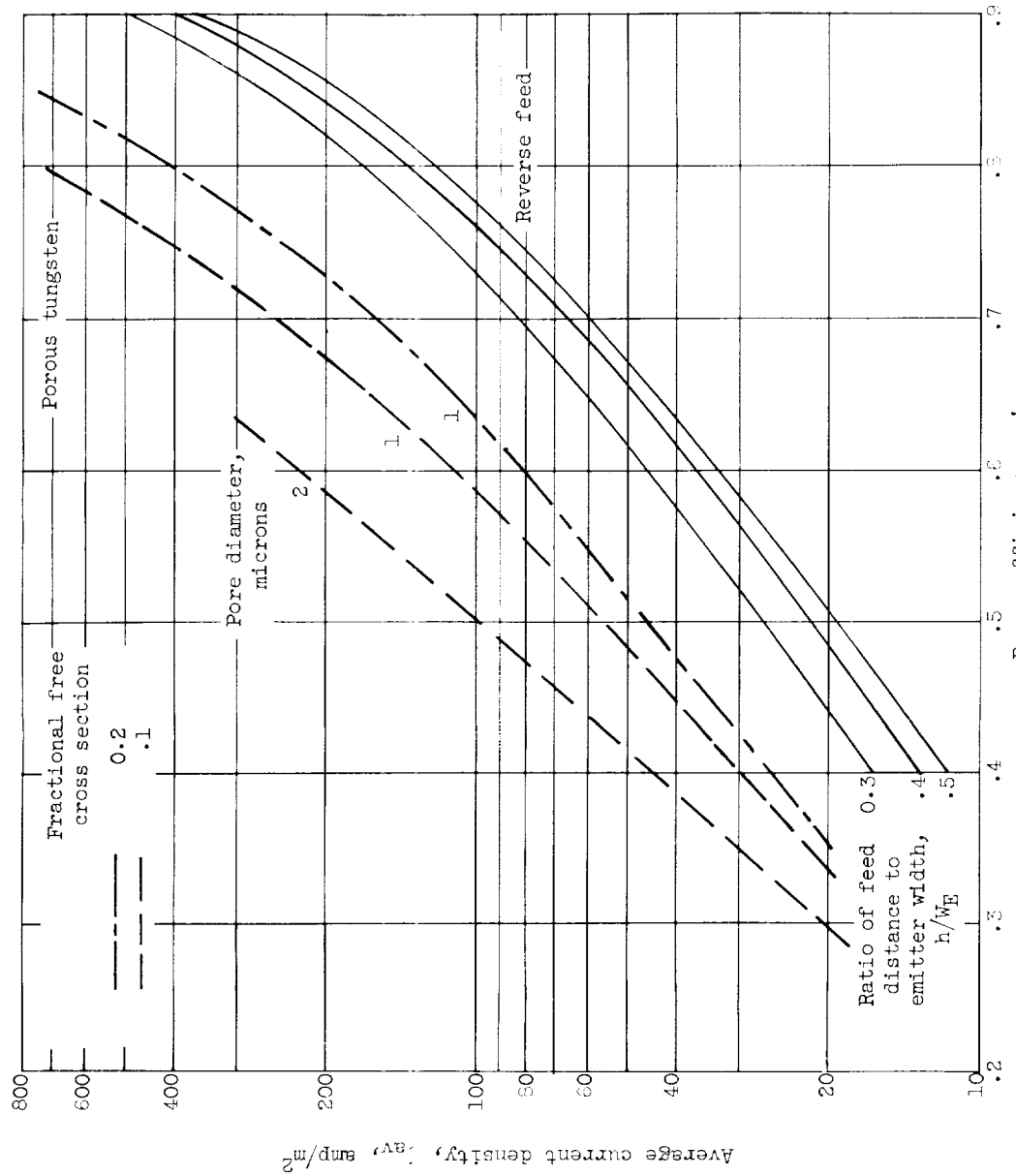

(b) Specific impulse, 5000 seconds.

Figure 6. - Continued. Variation of power efficiency with average current density.

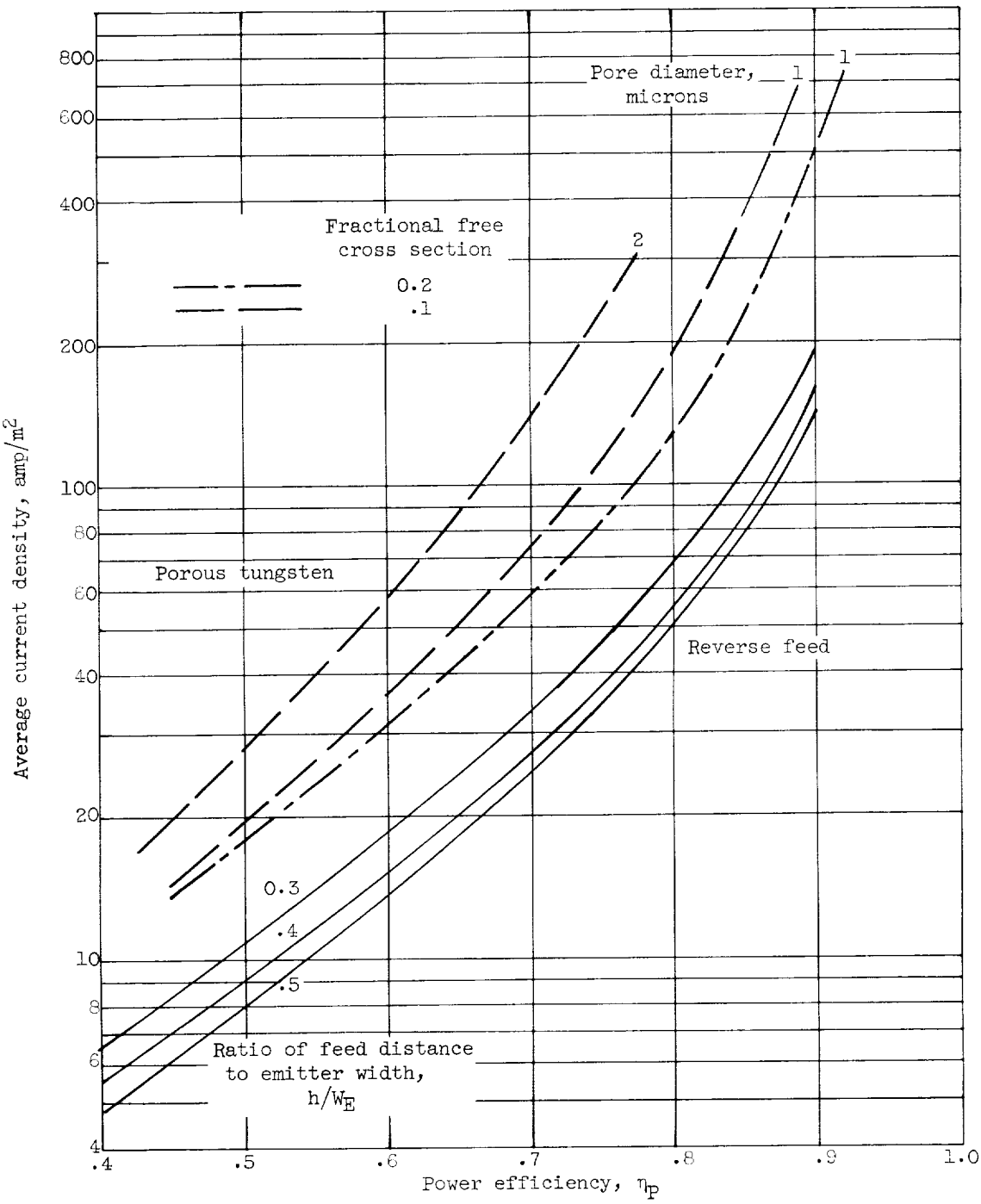

(c) Specific impulse, 7000 seconds.

Figure 6. - Continued. Variation of power efficiency with average current density.

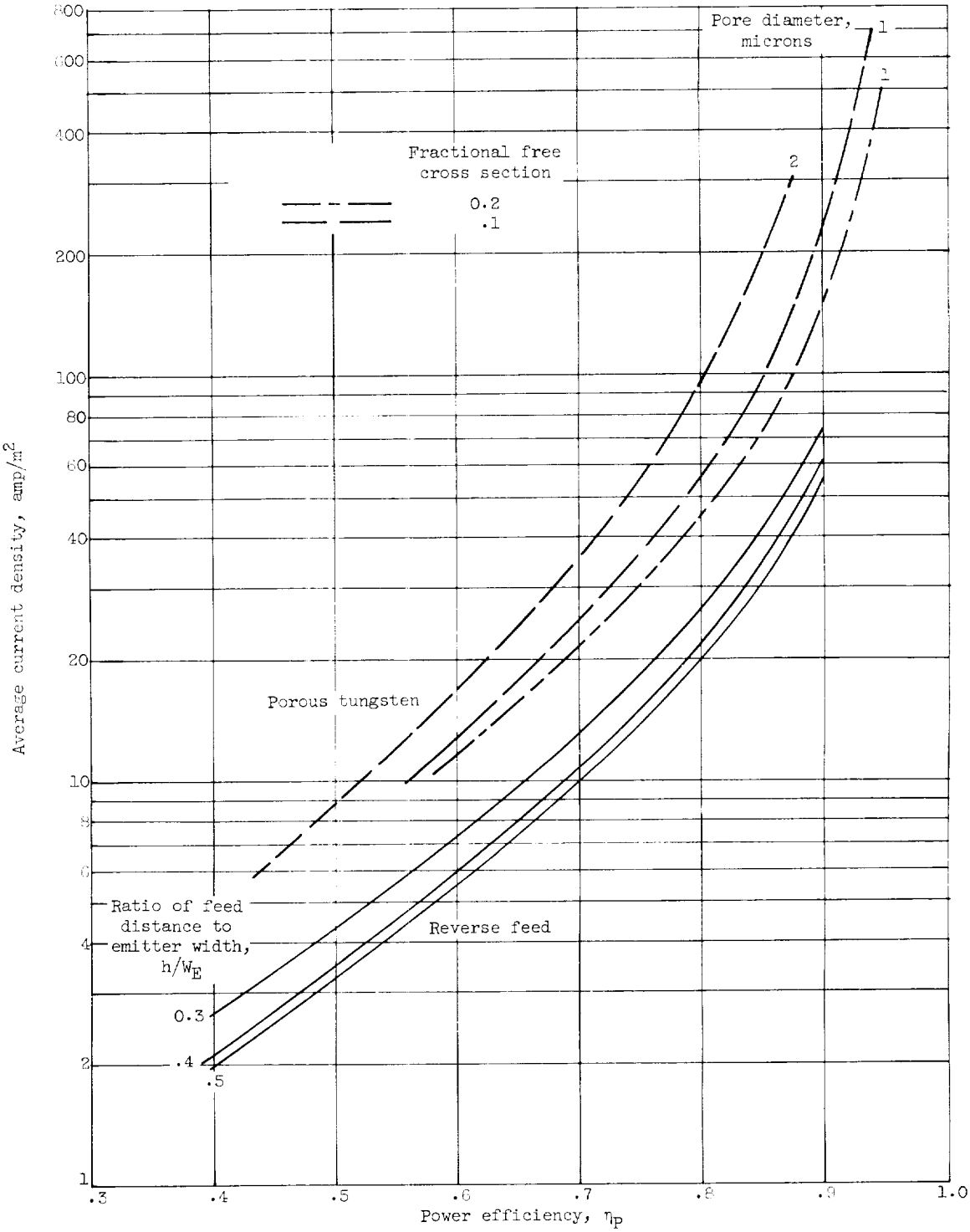

(d) Specific impulse, 10,000 seconds.

Figure 6. - Concluded. Variation of power efficiency with average current density.

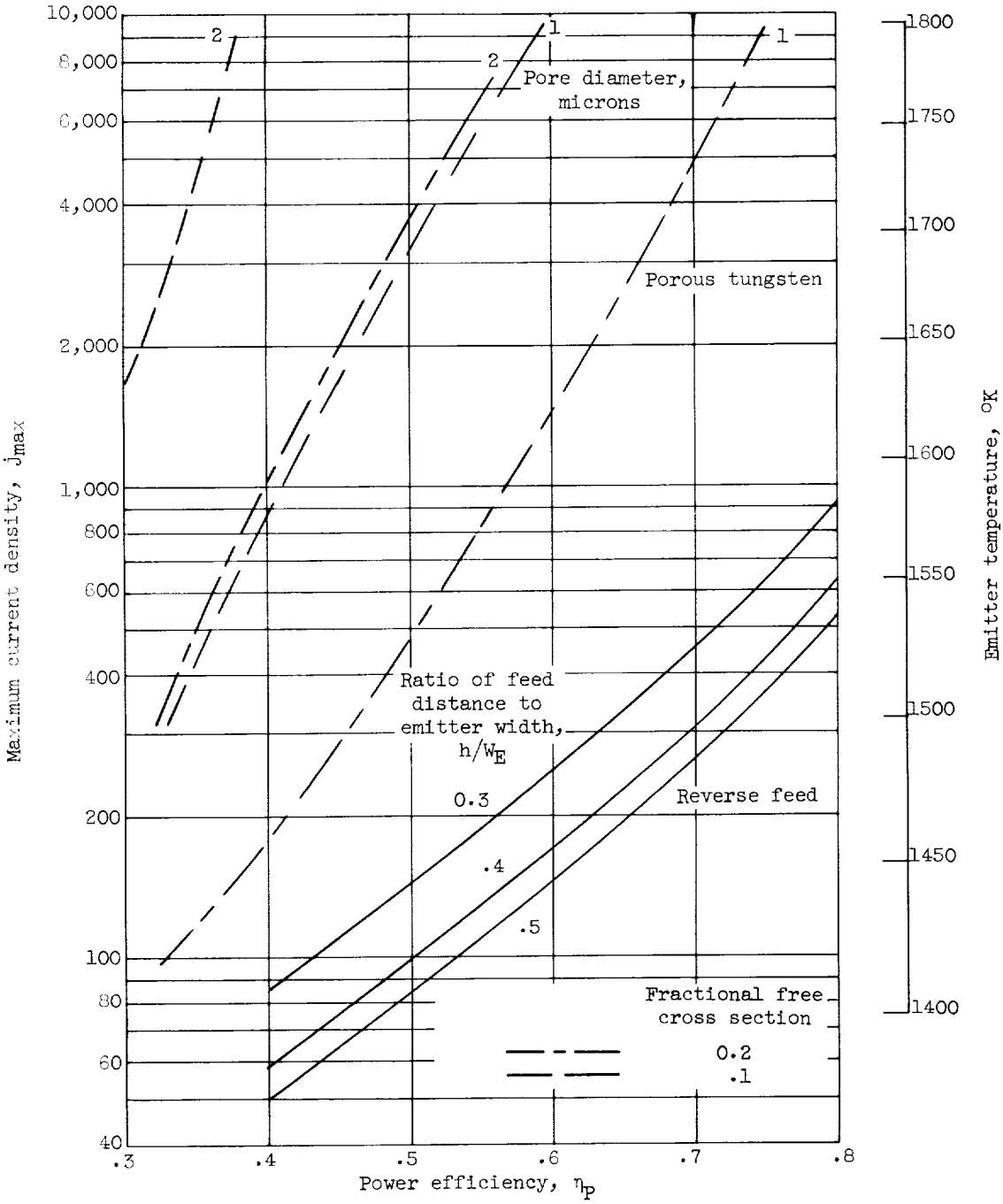

(a) Specific impulse, 3000 seconds.

Figure 7. - Variation of maximum current density and emitter temperature with power efficiency.

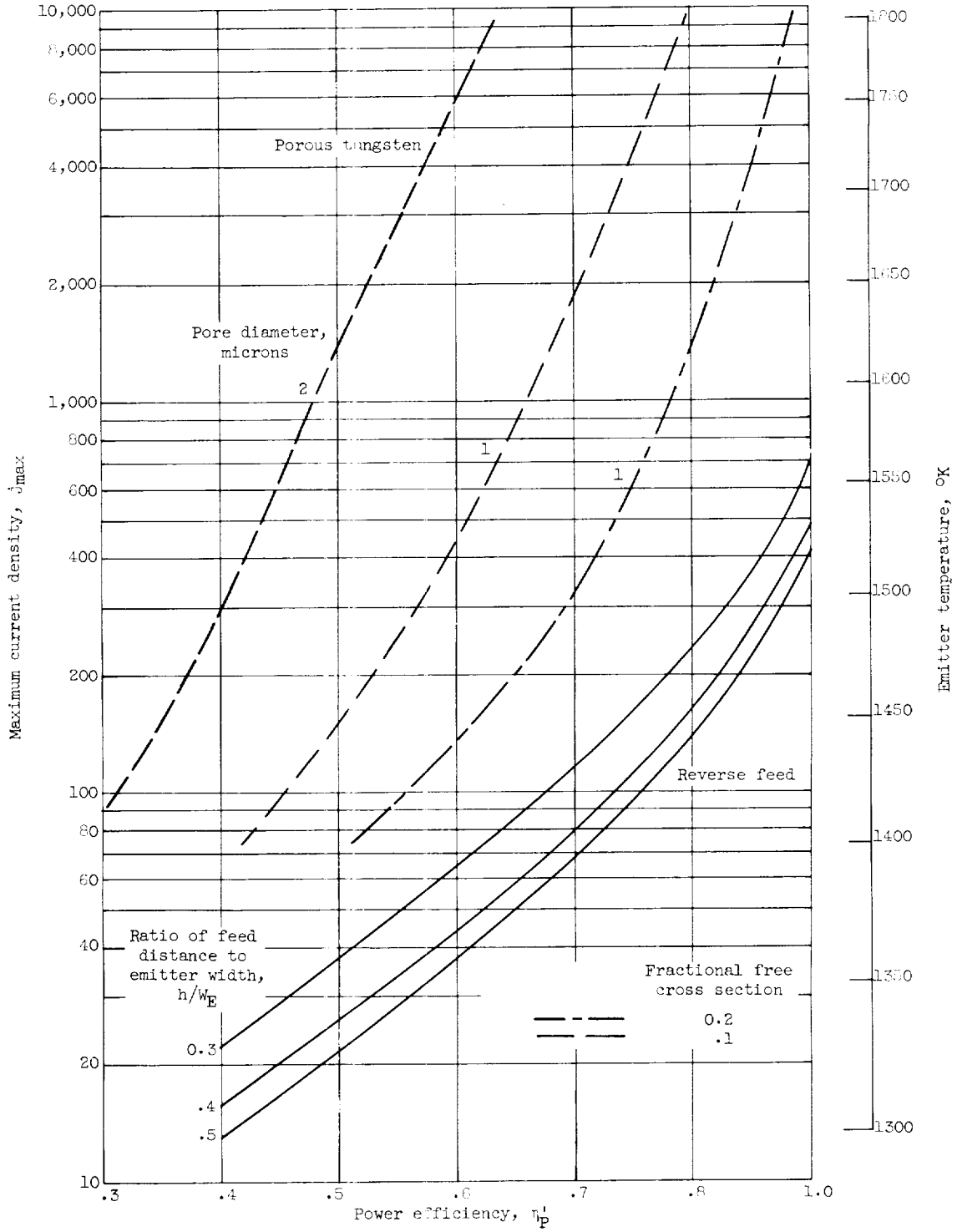

(b) Specific impulse, 5000 seconds.

Figure 7. - Continued. Variation of maximum current density and emitter temperature with power efficiency.

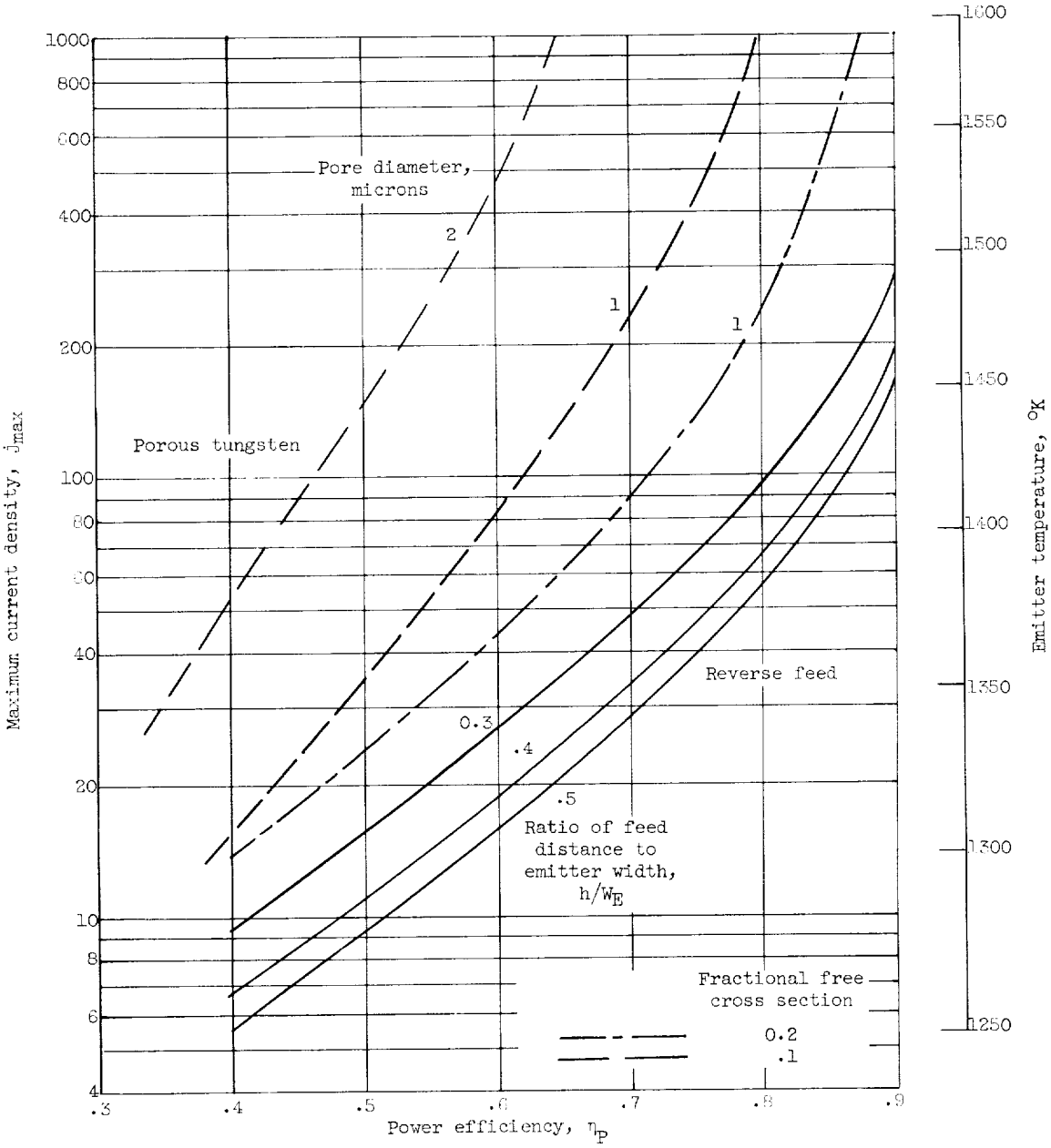

(c) Specific impulse, 7000 seconds.

Figure 7. - Continued. Variation of maximum current density and emitter temperature with power efficiency.

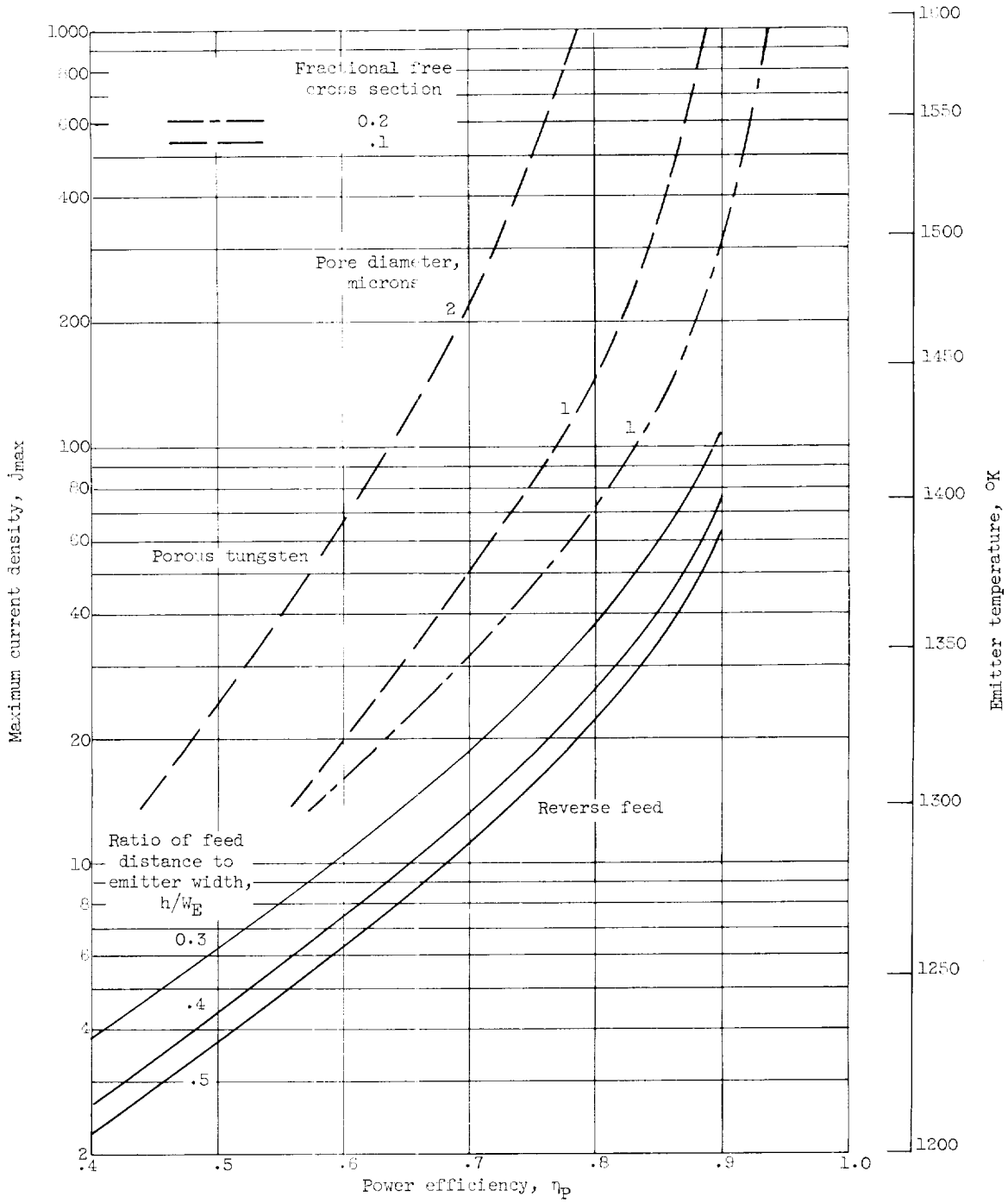

(d) Specific impulse, 10,000 seconds.

Figure 7. - Concluded. Variation of maximum current density and emitter temperature with power efficiency.

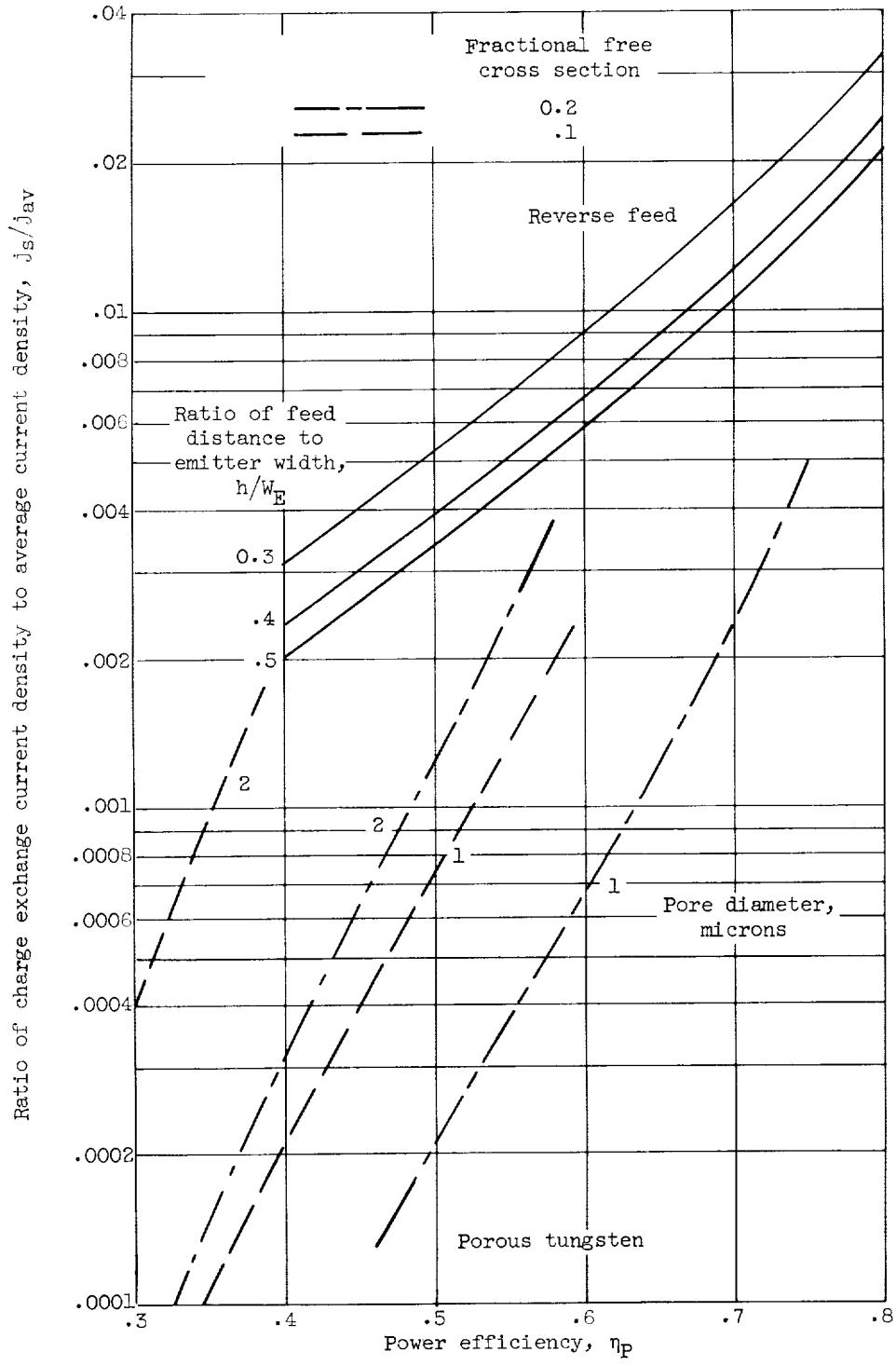

(a) Specific impulse, 3000 seconds.

Figure 8. - Variation of charge exchange currents with power efficiency.

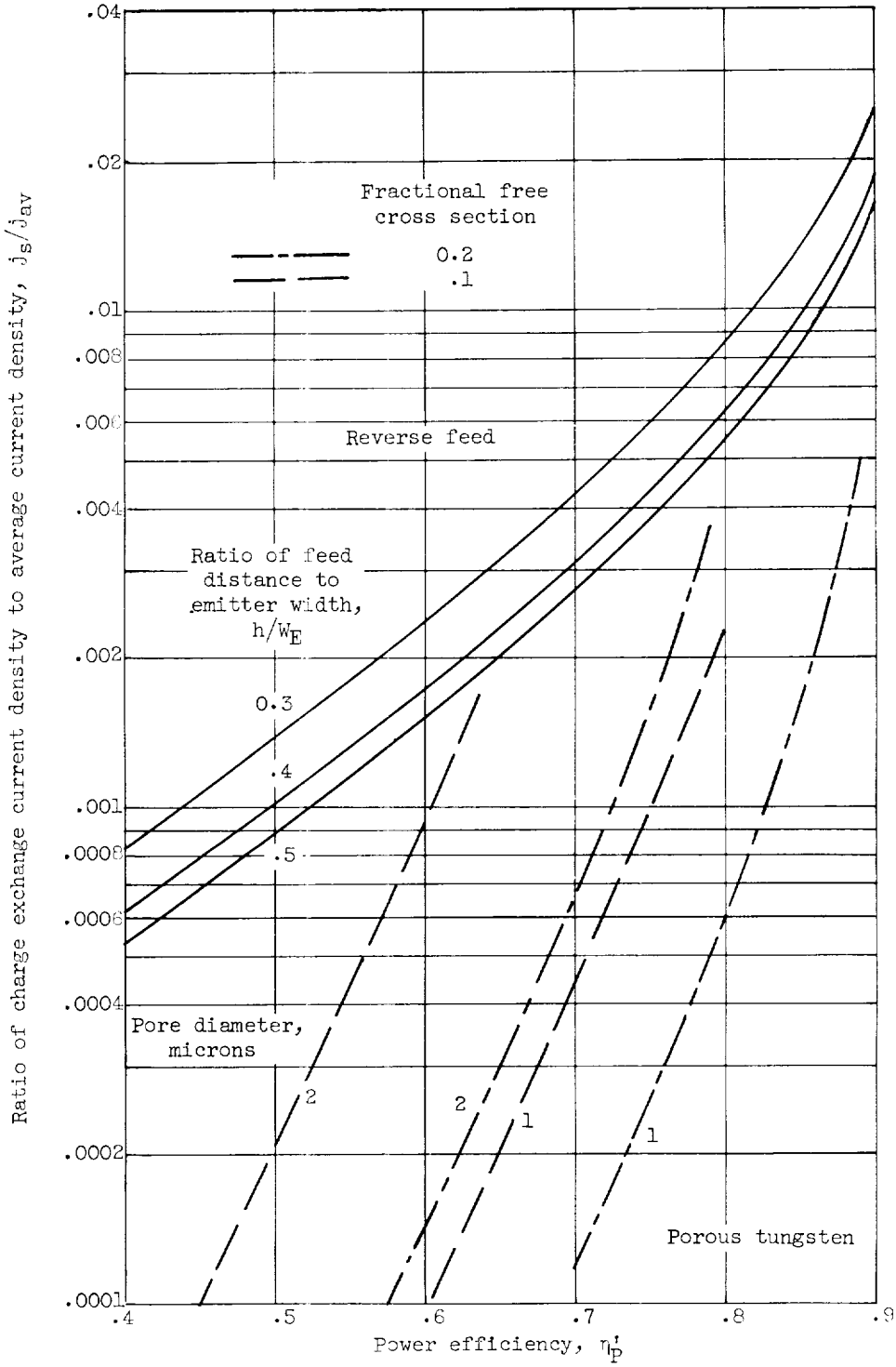

(b) Specific impulse, 5000 seconds.

Figure 8. - Continued. Variation of charge exchange currents with power efficiency.

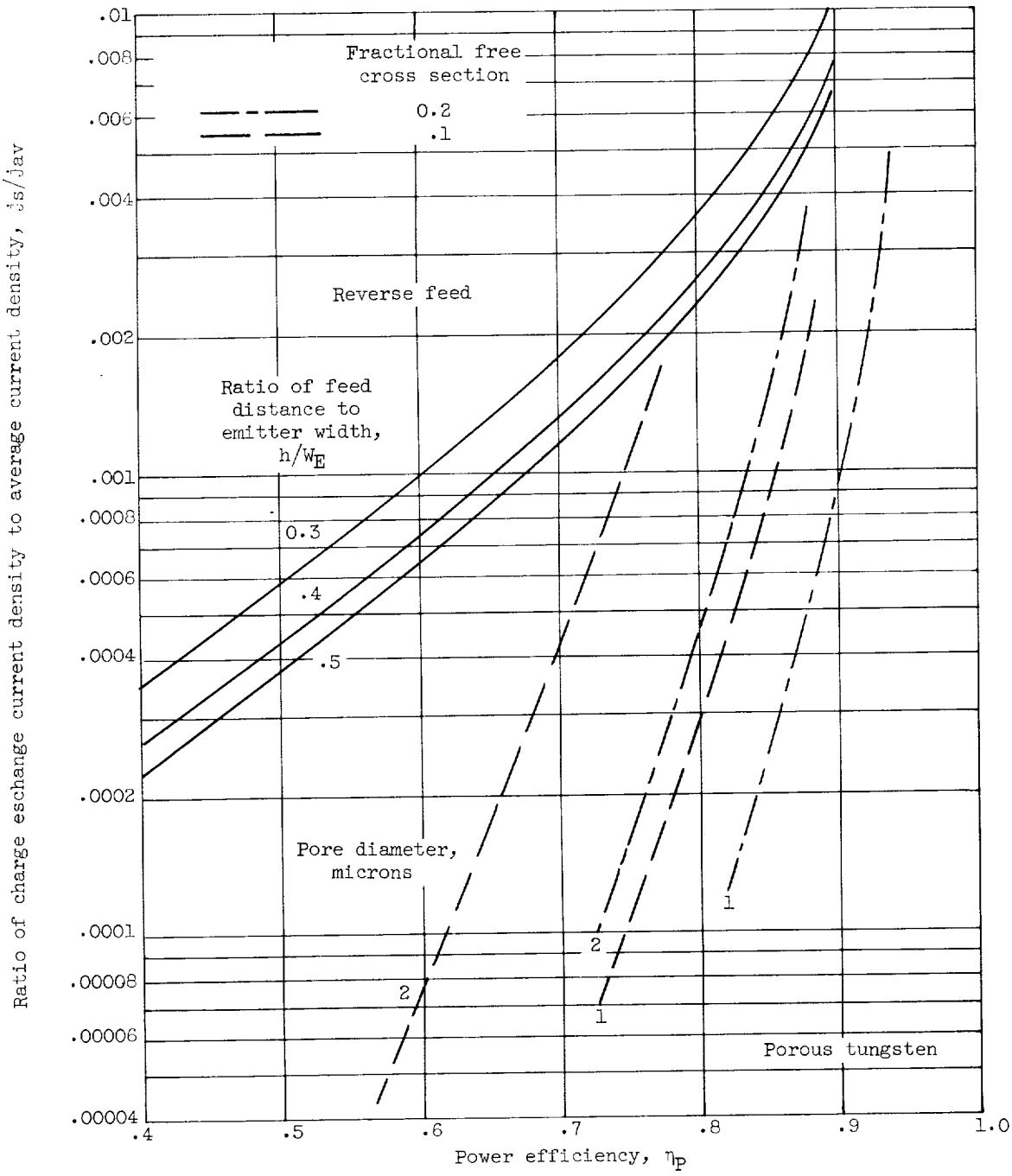

(c) Specific impulse, 7000 seconds.

Figure 8. - Continued. Variation of charge exchange currents with power efficiency.

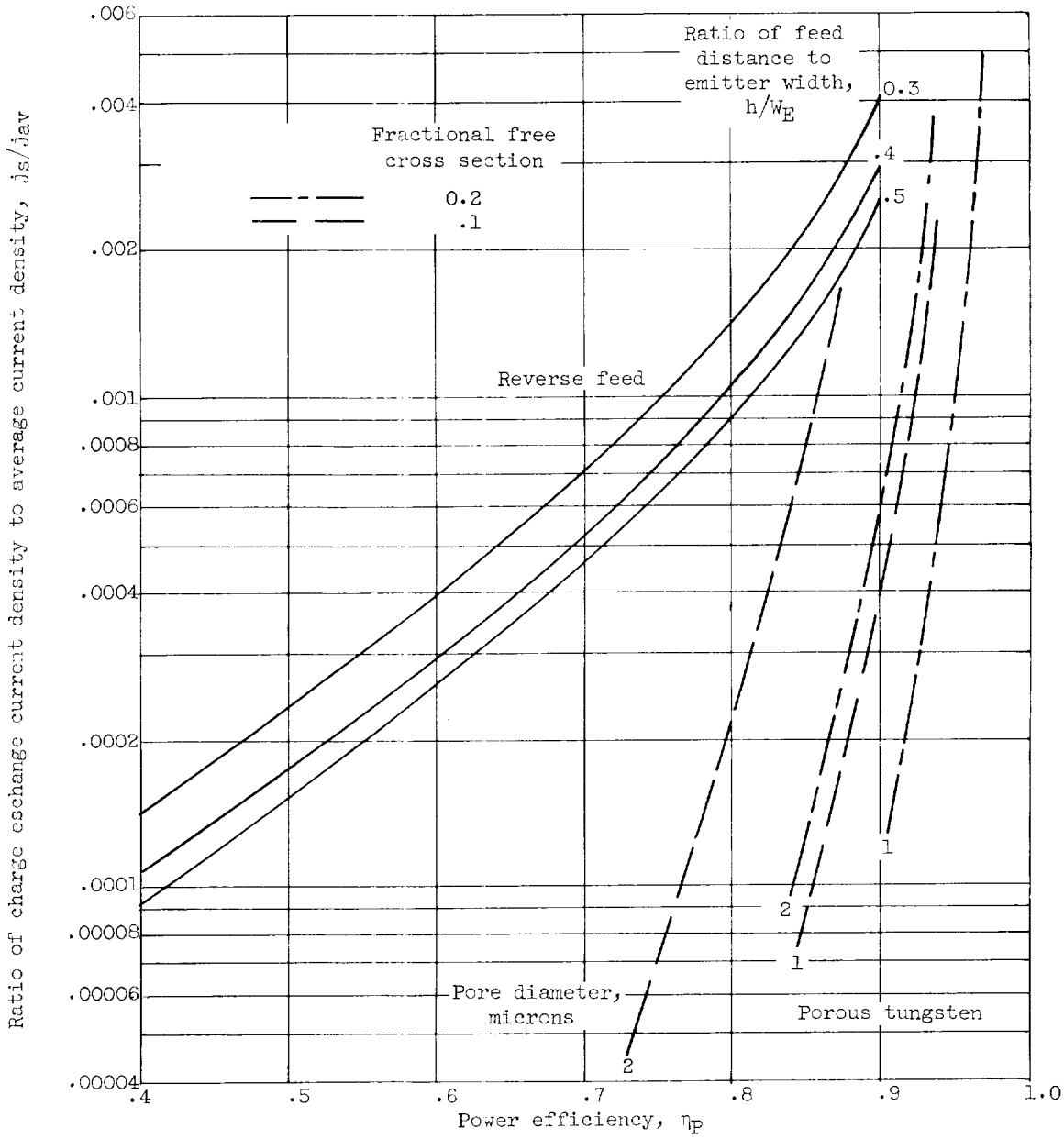

(d) Specific impulse, 10,000 seconds.

Figure 8. - Concluded. Variation of charge exchange currents with power efficiency.

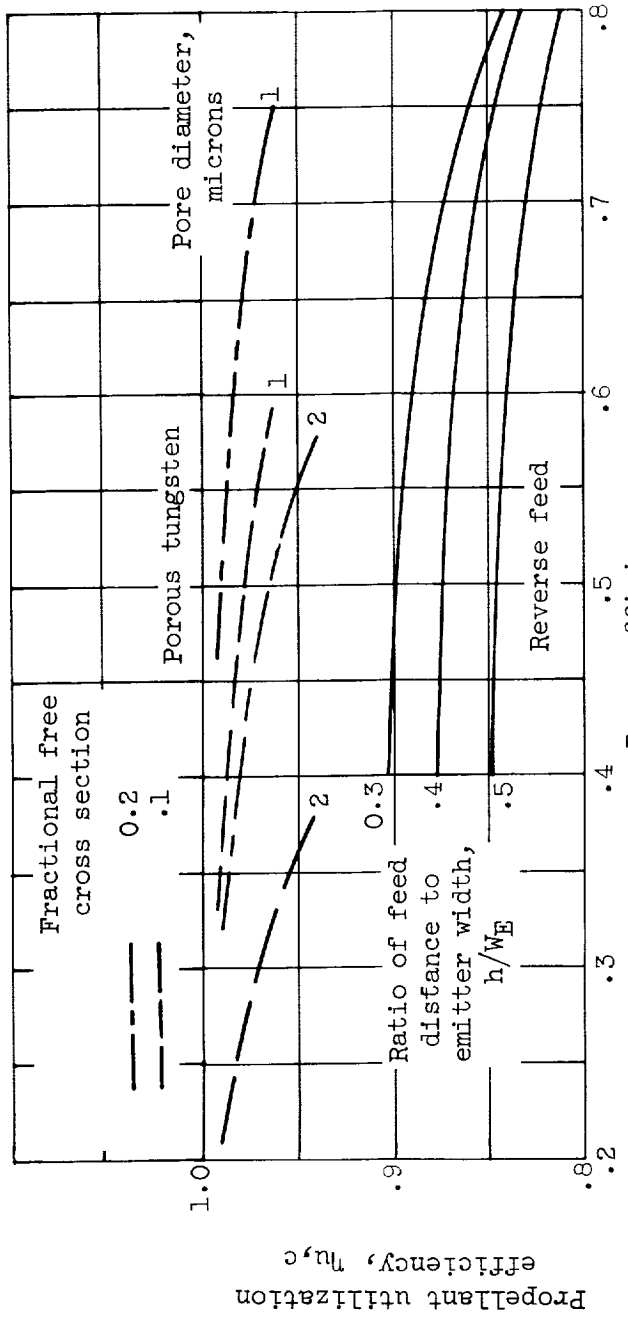

(a) Specific impulse, 3000 seconds.

Figure 9. - Variation of propellant utilization efficiency with power efficiency.

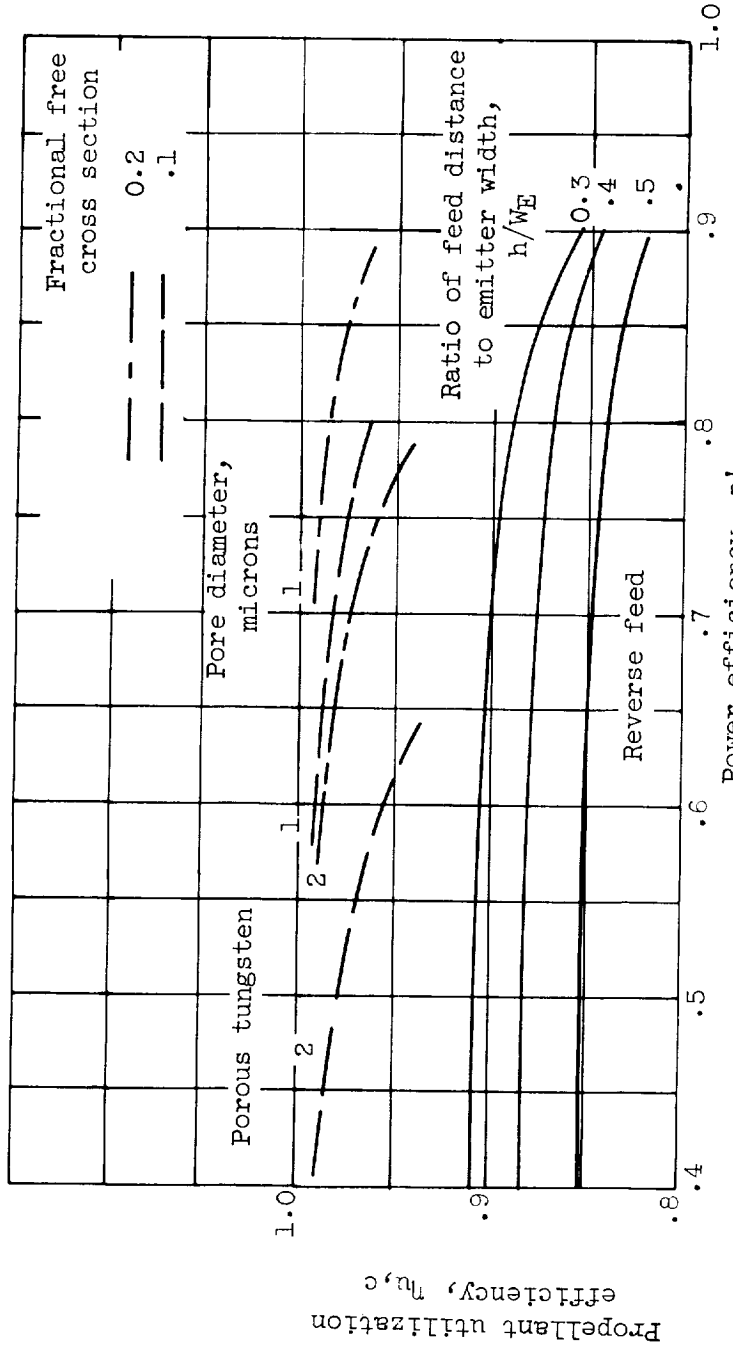

(b) Specific impulse, 5000 seconds.

Figure 9. - Continued. Variation of propellant utilization efficiency with power efficiency.

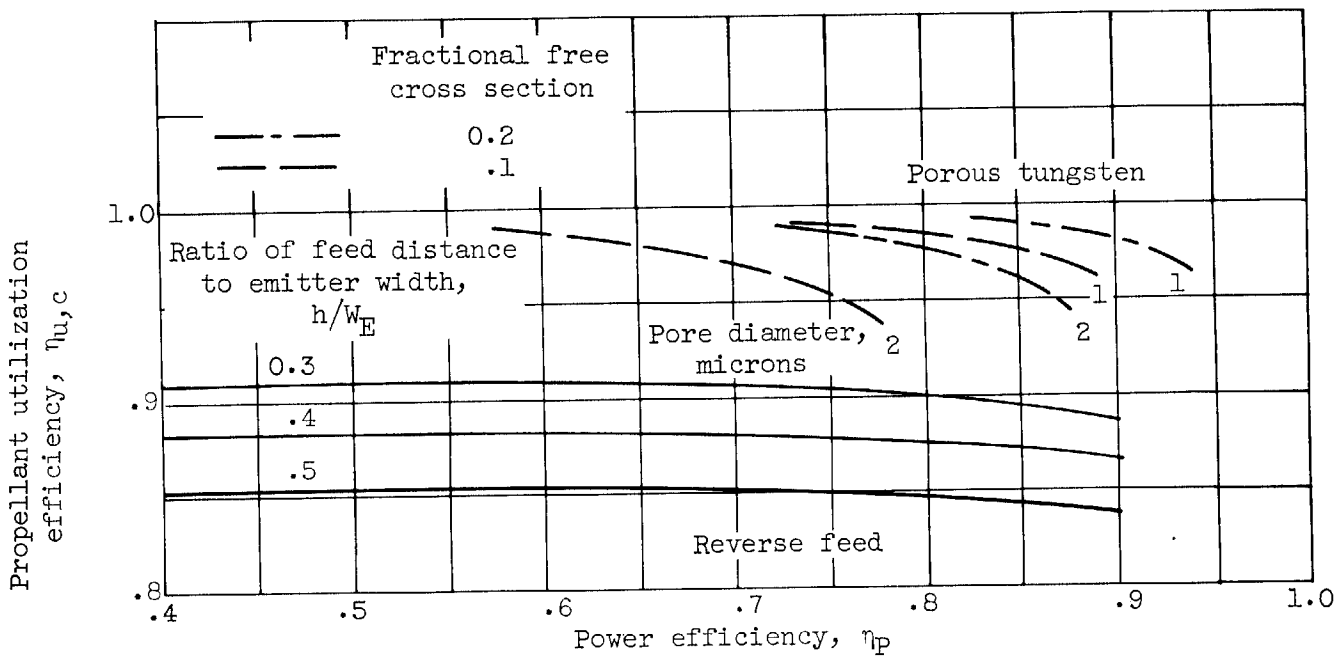

(c) Specific impulse, 7000 seconds.

Figure 9. - Continued. Variation of propellant utilization efficiency with power efficiency.

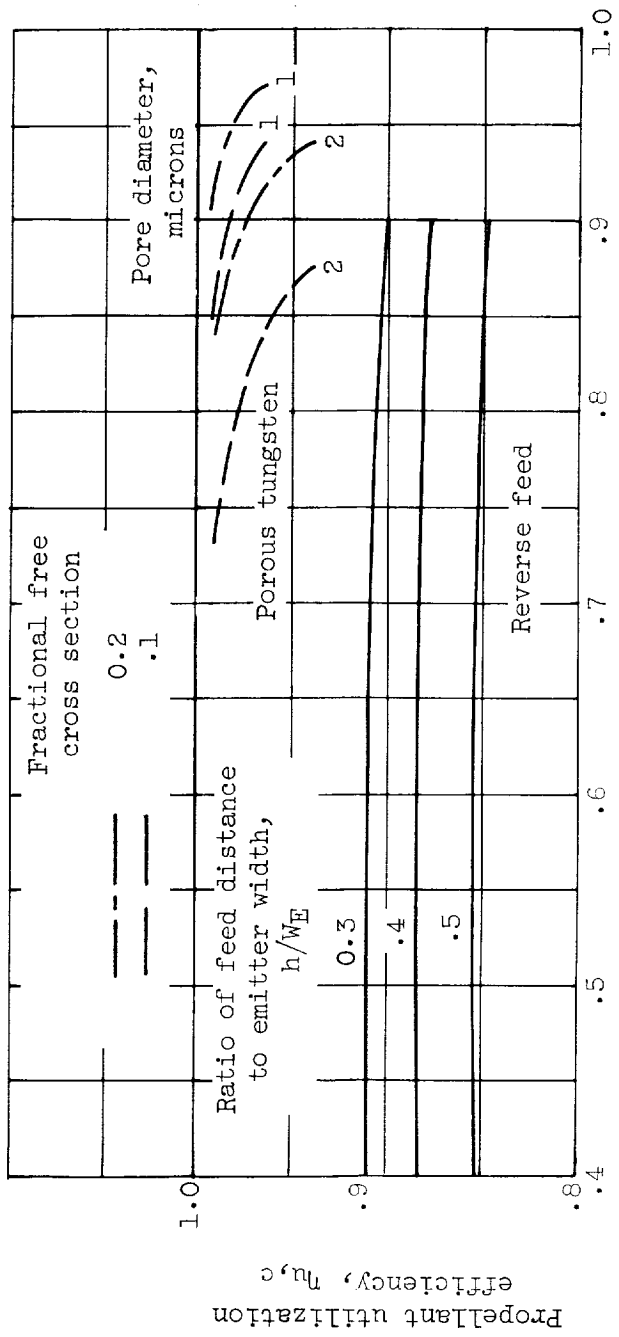

(d) Specific impulse, 10,000 seconds.

Figure 9. - Concluded. Variation of propellant utilization efficiency with power efficiency.